A Numerical Model of the Fluid Motion at a Density Front in the Presence of Background Turbulence

Y. NOH* AND H. J. S. FERNANDO

Department of Mechanical and Aerospace Engineering, Arizona State University, Tempe, Arizona

ABSTRACT

The effects of background turbulence on gravity currents produced by lock exchange are investigated using a numerical model with the aim of understanding the fluid motions associated with coastal fronts. It is shown that, at high turbulence intensities, the mutual intrusion of gravity currents is inhibited and the horizontal mass transport is dominated by the turbulent diffusion. The propagation of the front, the horizontal density flux, and the potential energy anomaly are calculated and are compared with available experimental data. The model is extended to include the effects of background rotation. It is found that, in the presence of background turbulence, the geostrophic equilibrium cannot be achieved, and the cross-frontal velocity persists indefinitely. The effects of rotation on the fluid motions were found to be impaired by the background turbulence.

1. Introduction

Generation of fronts is a common phenomenon in the ocean and atmosphere. Coastal regions, in particular, provide favorable conditions for the formation of fronts. For example, freshwater influx from river plumes can generate salinity fronts or salt wedges (Garvine and Monk 1974; Simpson and James 1986; McClimans 1988). Fronts also appear at the boundary between the well-mixed layer above the continental shelf and stratified waters away from the boundaries (Simpson et al. 1978). Formation of sea-breeze fronts is another example of front formation. As the cold air from the marine atmosphere undercuts the warm air mass over the land a sharp front, which can propagate as a gravity current, is developed. Additional examples of front formation in geophysical fluids can be seen in Scorer (1978) and Fedorov (1986).

Oceanic fronts are generally affected by the environmental turbulence generated by tidal mixing, heating and cooling, and mean-flow shear. When the intensity of the background turbulence is small, the front can retain a sharp density discontinuity and can propagate as a gravity current, whereas when the background turbulence is strong, the density front disappears and the horizontal mass transport occurs mainly by the turbulent diffusion. As an example, Fig. 1 shows the sa-

linity distribution in the main channel of the South San Francisco Bay, California. During neap tide, the tidal mixing is weak and the estuary is characterized by high stratification and a sharp front that separates the freshwater plume and background dense water. On the contrary, turbulent mixing during the spring tide is intense and the shelf water becomes vertically homogeneous thus impeding the frontogenesis.

To investigate the effects of background turbulence on gravity currents, several laboratory experiments have been carried out recently (Thomas and Simpson 1985; Linden and Simpson 1986; Noh and Fernando 1991, 1992). In particular, Linden and Simpson (1986) studied the effects of background turbulence on a gravity current that was generated using the lock-exchange flow configuration depicted in Fig. 2; a vertical barrier separating two fluids of different densities was removed to generate counterflowing gravity currents and the turbulence was generated by bubbling air from the base of the tank. It is found that transition occurs from the gravity current phase (characterized by a well-defined front) to the vertically mixed phase when $L_1/H \approx 0.08(BH)^{1/2}H/K$, where K is the turbulent diffusivity, $B (= g\Delta\rho/\rho_0$, where $\Delta\rho$ is the density difference, g is the gravitational acceleration, and ρ_0 is the reference density) is the buoyancy difference between the two fluids, H is the fluid depth, and L_1 is the distance over which the gravity current propagates before its destruction.

When the horizontal length scale of the front becomes large, the effects of the earth's rotation should be considered as well. The geostrophic adjustment inhibits the spreading of the front (or the cross-frontal velocity), and a coastal current develops parallel to the

* Current address: Dept. of Astronomy and Atmospheric Sciences, Yonsei University, Seoul, Korea.

Corresponding author address: Prof. H. J. Fernando, Department of Mechanical and Aerospace Engineering, Arizona State University, Tempe, AZ 85287-6106.
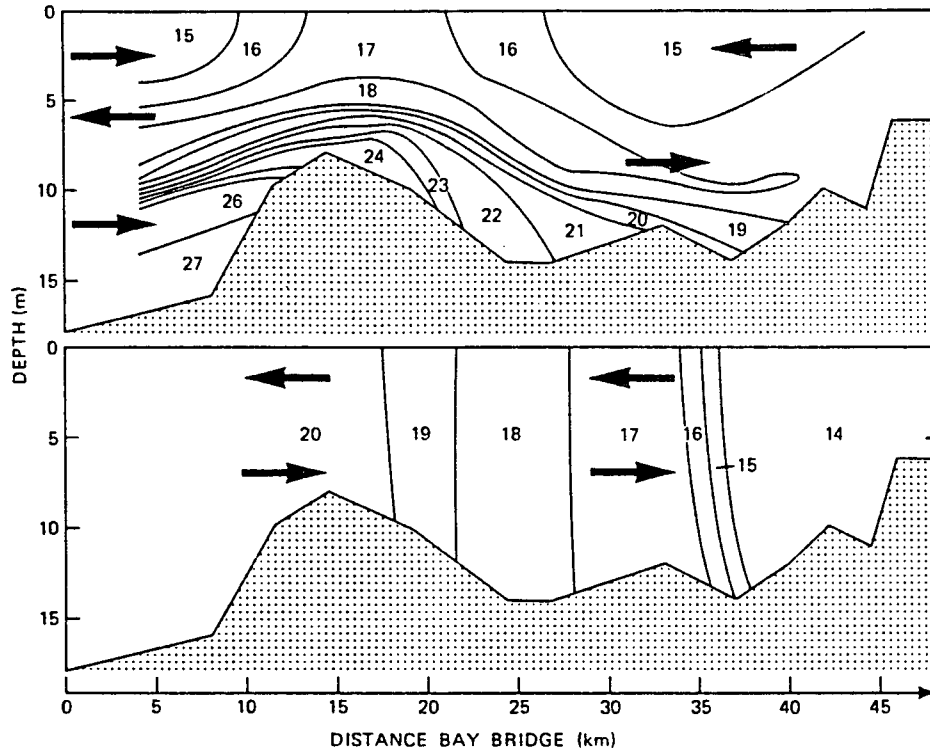
FIG. 1. Contours of salinity (ppt) along the main channel in South San Francisco Bay, California. Top: neap tide on 19 March 1982; bottom: spring tide on 26 March 1982. Arrows are inferred mean current directions (From Walters 1985).

front to facilitate the geostrophic equilibrium (Rossby 1937; Csanady 1971; Ou 1984; van Heijst 1985). This phenomenon has been well demonstrated by the laboratory experiments of Griffiths and Linden (1982) and Linden and van Heijst (1984). When a buoyant fluid is released in a rotating system, its front initially advances and then comes to an equilibrium at a distance corresponding to the Rossby radius of deformation λ ($\equiv (BH)^{1/2}/f$), where f is the Coriolis parameter.

As is evident from the studies of Simpson et al. (1978), the background turbulence plays an important role in the formation of tidal fronts since it determines whether the fluid layer is well mixed or stratified. The

FIG. 2. A sketch of the experimental apparatus of Linden and Simpson (1986).

effects of the eddy viscosity in such situations have been studied by Garrett and Loder (1981) and James (1981, 1984) using numerical models. Garrett and Loder (1981) showed that the eddy viscosity induces a cross-frontal velocity as a result of the interfacial friction between two fluids, but in their model the fluid was stratified and turbulent diffusion was neglected. James (1984) found that the amount of frontal sharpening and cross-frontal circulation patterns are sensitive to the magnitude of the eddy viscosity. No laboratory experiments have been performed so far to study the effects of background turbulence on the propagation of gravity currents in rotating fluids.

The purpose of this paper is to develop a two-dimensional numerical model to investigate the effects of background turbulence on gravity currents generated by lock exchange and to compare the results with the laboratory experimental results of Linden and Simpson (1986). The model is extended to include the effects of background rotation in order to investigate the effects of boundary mixing on geostrophic fronts. There have been several studies dealing with the numerical simulation of gravity currents (Daly and Pracht 1964; Wang 1984, 1985; Kao et al. 1977, 1978; Droegenmeier and Wilhelmson 1987; Haase and Smith 1989). In these studies, however, the effects of background turbulence have not been considered.
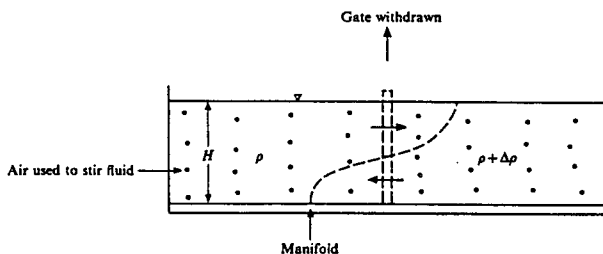
2. Model description

It is assumed that the gravity current is generated by the removal of a vertical barrier at the center of a tank of horizontal scale L and vertical scale H; see Fig. 2. The barrier initially separates two water masses between which there is a density difference $\Delta\rho$. The eddy viscosity K is assumed to be constant throughout the tank, and is determined by the background turbulence level. In the experiments of Linden and Simpson (1986), the turbulence was generated by rising bubbles and the resulting turbulence was regarded as approximately uniform throughout the depth of the fluid; this justifies the use of constant eddy diffusivity in the present work. However, if the turbulence is significantly affected by the shear stresses or the stratification, this assumption needs to be modified. The turbulent Prandtl number of the fluid is assumed to be unity.

Using H, B, U $[\equiv(BH)^{1/2}]$ and T $(\equiv H/U)$ as the scales for length, buoyancy, velocity, and time, respectively, the nondimensionalized governing equations for an incompressible, turbulent, two-dimensional flow can be written as[1]

$$\frac{\partial u}{\partial t} + \frac{\partial}{\partial x}(uu) + \frac{\partial}{\partial z}(uw) - Fv$$

$$= -\frac{1}{\rho_0}\frac{\partial p}{\partial x} + R\left(\frac{\partial^2 u}{\partial x^2} + \frac{\partial^2 u}{\partial z^2}\right), \quad (2.1)$$

$$\frac{\partial w}{\partial t} + \frac{\partial}{\partial x}(uw) + \frac{\partial}{\partial z}(ww)$$

$$= -\frac{1}{\rho_0}\frac{\partial p}{\partial z} + R\left(\frac{\partial^2 w}{\partial x^2} + \frac{\partial^2 w}{\partial z^2}\right) - b, \quad (2.2)$$

$$\frac{\partial u}{\partial x} + \frac{\partial w}{\partial z} = 0, \quad (2.3)$$

$$\frac{\partial v}{\partial t} + \frac{\partial}{\partial x}(uv) + \frac{\partial}{\partial z}(vw) + Fu$$

$$= R\left(\frac{\partial^2 v}{\partial x^2} + \frac{\partial^2 v}{\partial z^2}\right), \quad (2.4)$$

$$\frac{\partial b}{\partial t} + \frac{\partial}{\partial x}(ub) + \frac{\partial}{\partial z}(wb) = R\left(\frac{\partial^2 b}{\partial x^2} + \frac{\partial^2 b}{\partial z^2}\right), \quad (2.5)$$

where homogeneity is assumed in the y direction. Here x and y are the longitudinal and transversal directions to the front and z is the vertical direction; u, v, and w are the corresponding mean velocities; p is the mean

---

[1] Unless otherwise stated, the variables are nondimensional. The dimensional equations are denoted by an asterisk (*).

pressure; and b is the mean buoyancy. The parameters R and F are defined by

$$R = \frac{K}{(BH)^{1/2}H} \quad (2.6)$$

and

$$F = \frac{f}{(B/H)^{1/2}}, \quad (2.7)$$

where f is the Coriolis parameter.

Equations (2.1)–(2.3) can be rewritten in terms of the streamfunction and vorticity as

$$\frac{\partial \zeta}{\partial t} + \frac{\partial}{\partial x}(u\zeta) + \frac{\partial}{\partial z}(w\zeta) - F\frac{\partial v}{\partial z}$$

$$= -\frac{\partial b}{\partial x} + R\nabla^2\zeta, \quad (2.8)$$

$$\nabla^2\psi = \zeta, \quad (2.9)$$

where ζ and ψ are dimensionless vorticity and streamfunction, respectively, defined by

$$\zeta = \frac{\partial u}{\partial z} - \frac{\partial w}{\partial x}, \quad (2.10)$$

$$u = \frac{\partial \psi}{\partial z} \quad w = -\frac{\partial \psi}{\partial x}. \quad (2.11)$$

The initial conditions are

$$b = \begin{cases} 1, & -a/2 < x < 0 \\ 0, & 0 \leq x < a/2, \end{cases} \quad (2.12)$$

$$\psi = 0, \quad (2.13)$$

$$v = 0, \quad (2.14)$$

where $a = L/H$. In other words, initially two homogeneous fluids at rest are separated by a vertical barrier located at $x = 0$. In the calculations, $a = 15$ was used, corresponding to the experiment of Linden and Simpson (1986).

In the model, the bottom friction is parametrized by

$$\tau_{bx}\left(= K\frac{\partial u}{\partial z}\bigg|_{z=0}\right) = C_D u^* u_b, \quad (2.15)$$

$$\tau_{by}\left(= K\frac{\partial v}{\partial z}\bigg|_{z=0}\right) = C_D u^* v_b, \quad (2.16)$$

where $u_b = u(z = 0)$, $v_b = v(z = 0)$, and $u^* = (u_b^2 + v_b^2)^{1/2}$. In the oceanic context, the typical value of the friction coefficient is known to be $C_D = 2 \times 10^{-3}$ (Blumberg and Mellor 1987; Bowden 1983; Ramming and Kowalik 1980). In the present simulations various bottom boundary conditions were employed and the

results were compared with the laboratory experimental results of Linden and Simpson (1986); however, the satisfactory agreement between the two was still found when $C_D = 2 \times 10^{-3}$ (see section 3a for discussion), and hence this value was used for the rest of the calculations. The water surface was considered as stress-free, and zero buoyancy flux condition across all boundaries was assumed for b.

A finite-difference scheme was used for the numerical solution, where the advection terms are calculated explicitly and the diffusion terms are calculated implicitly using the ADI method. A uniform grid size was used in both horizontal and vertical directions; namely, $\Delta x = 0.05$ and $\Delta z = 0.01$. The fields of density and velocity were evaluated after each iteration, and convergence of the solution of the elliptic equation (2.9) was verified using the test

$$\Delta \psi_{max} < 10^{-5}, \qquad (2.17)$$

where $\Delta \psi_{max}$ is the maximum difference between ψ values corresponding to consecutive iterations. The numerical scheme used was similar to that used by Kao et al. (1978) for simulation of gravity currents.

The truncation error, which leads to the numerical diffusion in solving the vorticity equation (2.8), can be estimated as $ND = (|u|\Delta x/2)\partial^2\zeta/\partial x^2 + (|w|\Delta z/2)\partial^2\zeta/\partial x^2$ (Kao et al. 1978). Similar numerical diffusion exists for the case of the density equation (2.5). To ensure numerical accuracy of the computational results, it was necessary to compare the magnitude of this truncation error with the advective term $AD \equiv \partial(u\zeta)/\partial x + \partial(w\zeta)/\partial z$ and the physical diffusion term $PD \equiv R\nabla^2\zeta$ at various points in the flow field. The error estimates were obtained in terms of AD/ND and PD/ND throughout the flow field, over the entire range of R used ($0.01 < R < 0.1$). The results showed that $AD/ND \sim 10 - 10^2$ and $PD/ND \sim 10 - 10^4$, suggesting that the numerical diffusion has not obscured the physics of the problem.

3. Results

a. Nonrotating case

The density distributions and the streamfunctions are shown in Figs. 3 and 4, for the cases $R = 0.01$ and 0.1, respectively, for $t = 5$. When $R = 0.01$ (Fig. 3), they are similar to those observed during typical lock exchange flows and take the form of mutually intruding gravity currents with sharp fronts (Simpson 1987). On the other hand, when $R = 0.1$ (Fig. 4), the density distribution characterizes a pattern that is produced by turbulent diffusion only. The streamfunctions reveal a weaker circulation compared to the previous case.

Figure 5a shows the propagation of the density front when $R = 0.02$. Here the frontal position (x_f, z_f) is defined as the position where the isopycnal contour B
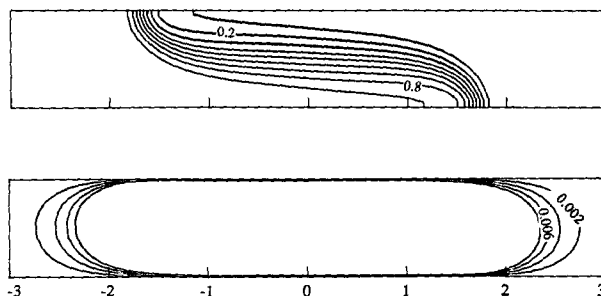

FIG. 3. (a) The density distribution $b(x, z)$: $t = 5$, $R = 0.01$. (b) The streamlines of the flow $\psi(x, z)$: $t = 5$, $R = 0.01$.

$= 0.1$ shows its maximum x. The results indicated that, for the value of C_D used, x_f always occurs at the bottom surface ($z_f = 0$). The data from the experiments of Linden and Simpson (1986), with $R = 0.17, 0.19$, and 0.26, are also shown for comparison. The broken line indicates the slope corresponding to the propagation of a gravity current in nonturbulent surroundings (Simpson 1987), namely,

$$x_f = 0.46t. \qquad (3.1)$$

Tests were carried out with different bottom boundary conditions specified by different bottom-drag coefficients, and the results are shown in Fig. 5b. Note that the results are not very sensitive to the value of C_D, except that the no-slip boundary condition yields significantly lower results compared to either the $C_D = 2 \times 10^{-3}$ case or to the experimental results. This is in agreement with Haase and Smith (1989), who found that the calculations based on the no-slip condition at the bottom underestimate the gravity current velocity.

Figure 6 shows the variation of the frontal position with time for different R values. The front propagation appears to be slowed down with increasing R as a result of the increase in eddy viscosity and the decrease of horizontal density gradient. Although this observation is in agreement with the experimental results of Linden and Simpson (1986), a sudden deviation from (3.1), which they reported to have observed in the experiments (see Fig. 5a), could not be identified here. A distinct transition from the gravity current regime to the vertically mixed regime could not be found either from the time evolution records of the density distribution such as Fig. 3a. Instead, as x_f increases, the deviation from (3.1) due to background turbulence was observed to be rather gradual, as is evident from Fig. 5a.

It is important, however, to note that in laboratory situations turbulence is generated at the frontal region of the gravity current as a result of instabilities, and at small R the intensity of this turbulence can be stronger than that of the imposed ambient turbulence. This aspect is not accounted for in the numerical simulation, where only the externally imposed turbulence was
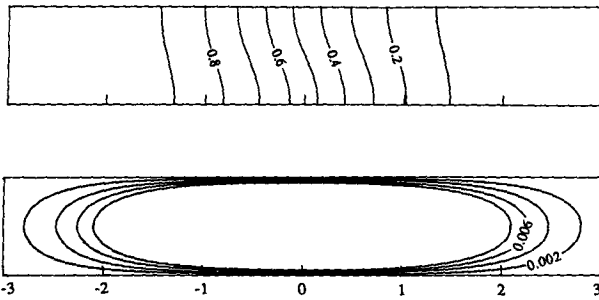
FIG. 4. (a) The density distribution $b(x, z)$: $t = 5$, $R = 0.1$.
(b) The streamlines of the flow $\psi(x, z)$: $t = 5$, $R = 0.1$.

considered. This internally generated turbulence and resulting mixing in the frontal region help to maintain a sharp front and a large horizontal pressure gradient across the front, until the frontal processes are dominated by the background turbulence. This may account for the differences in the observations made in the numerical simulations and in the laboratory with regard to the transition from the gravity current–dominated regime to the turbulent diffusion–dominated regime.

The frontal thickness of the gravity current δ was estimated based on the definition $\delta = x_f^+ - x_f^-$, where $B(x = x_f^+, z = z_f) = 0.1 \pm 0.05$. The results are shown in Fig. 7 for different values of R. When $R \leqslant 0.02$, a relatively sharp front with a constant thickness is maintained during the propagation. On the other hand, when $R \geqslant 0.08$, the increase of δ is characterized by turbulent diffusion so as to yield $\delta \sim (Rt)^{1/2}$.

The stratification within the fluid can be quantified as a potential energy anomaly ϕ, which represents the amount of energy required to restore the vertically mixed condition (Simpson 1981),

$$\phi = \int_0^1 (\bar{b} - b) z dz, \qquad (3.2)$$

where $\bar{b}$ is the depth-averaged mean buoyancy. The variation of $\phi(x = 0)$ with time is shown in Fig. 8 for different values of R. Note the generation of stratification at the onset of the lock–exchange process and its destruction with time depending on the intensity of the background turbulence.

The horizontal density flux (integrated over the water depth) Q can be determined by using

$$\frac{\partial \bar{b}}{\partial t} = -\frac{\partial Q}{\partial x}. \qquad (3.3)$$

Here the vertically integrated value of b is represented by $\bar{b}$ in view of $H = 1$. Its value at the center $Q_0 [\equiv Q(x = 0)]$ is then obtained by

$$Q_0 = -\int_{-a/2}^0 \frac{\partial \bar{b}}{\partial t} dx, \qquad (3.4)$$

using $Q(x = -a/2, R) = 0$.

Figure 9 shows the variations of Q_0 with time for different R values. If the advection owing to gravity currents is dominant, then Q is expected to be characterized by their velocities: that is, a rapid acceleration to their maximum and then a slow deceleration. On
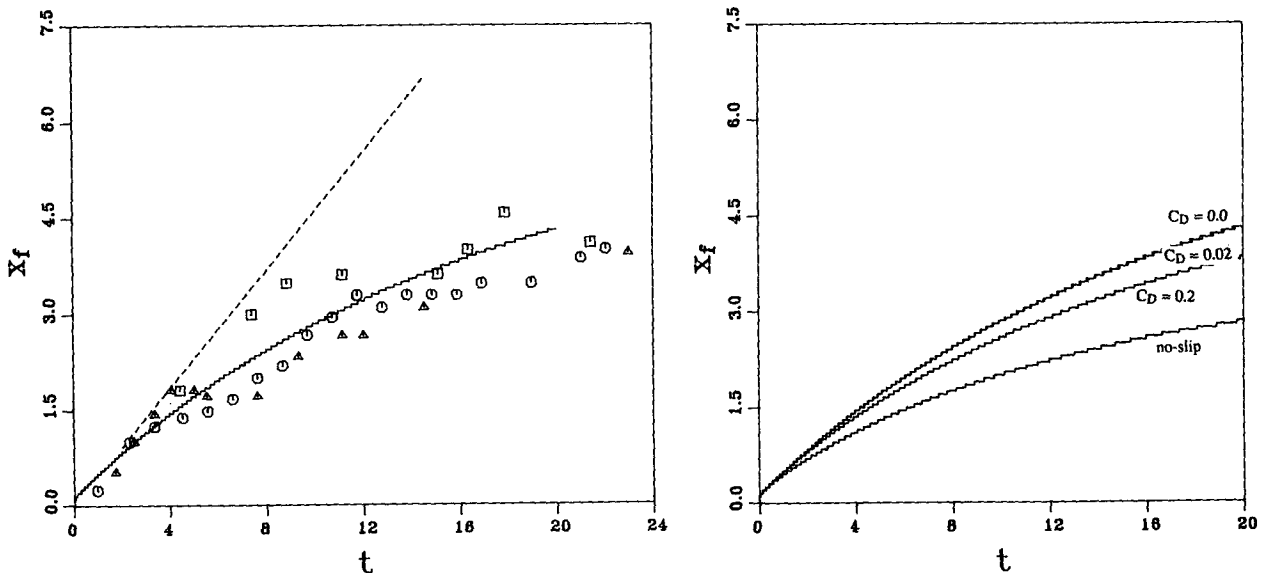

FIG. 5. (a) The propagation of the frontal position x_f with time when $R = 0.02$; here x_f is defined by the maximum x of $B = 0.1$ contour. The broken line indicates the corresponding results without background turbulence ($R = 0$), $x_f = 0.46t$. The experimental data are from Linden and Simpson (1986): □, $R = 0.17$; ○, $R = 0.19$; △, $R = 0.26$. (b) The propagations of x_f with time for different bottom boundary conditions, that is, C_D values, when $R = 0.02$. The results with $C_D = 0.0$ and $C_D = 0.02$ are almost identical.
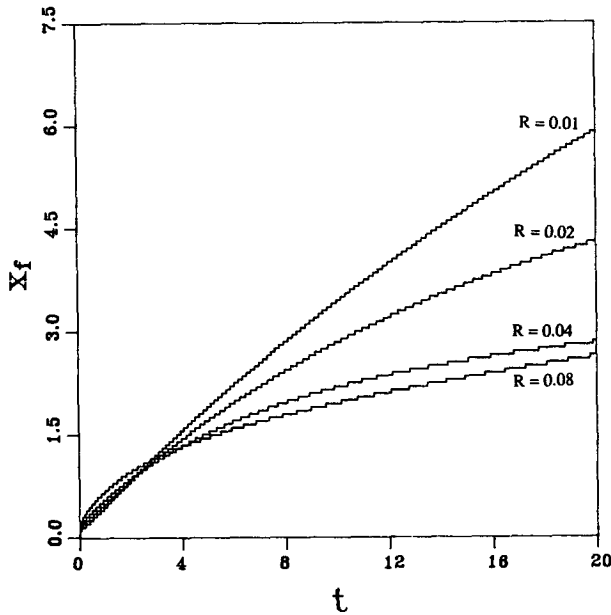
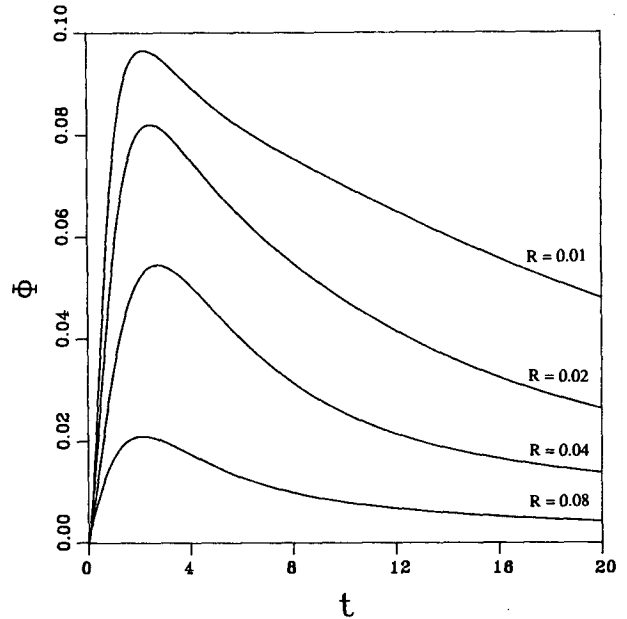FIG. 6. The propagation of the front x_f with time t for different R.

FIG. 8. The variation of potential energy anomaly ϕ with time for different R.

the other hand, when the turbulent diffusion is dominating, Q is expected to be a monotonically decreasing function of time. Thus, it is possible to suggest that the advection by the gravity current is important when $R < 0.04$ (*gravity current regime*), but the turbulent diffusion dominates when $R > 0.08$ (*turbulent diffusion regime*). It was also found that Q_0 decreases with R in the gravity current regime, but increases with R in the turbulent diffusion regime.

It is of interest to investigate the case where the horizontal buoyancy transport occurs solely by diffusion (i.e., as a Fickian process). In this case, the dimensional buoyancy conservation law can be written as

$$\frac{\partial \bar{b}}{\partial t} = K \frac{\partial^2 \bar{b}}{\partial x^2}, \qquad (3.5)^*$$
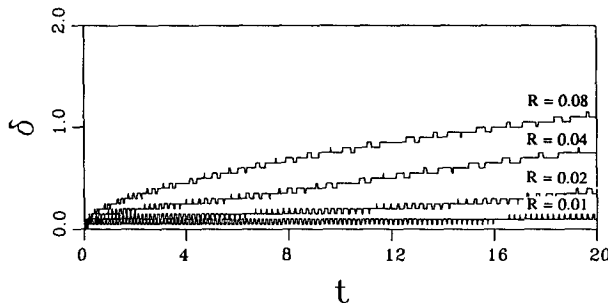
and Q_0 can be related to K from (3.4) as

$$Q_0 = -KH \left(\frac{\partial \bar{b}}{\partial x} \right)_{x=0}. \qquad (3.6)^*$$

FIG. 7. The variation of the frontal thickness δ with time t for different R.
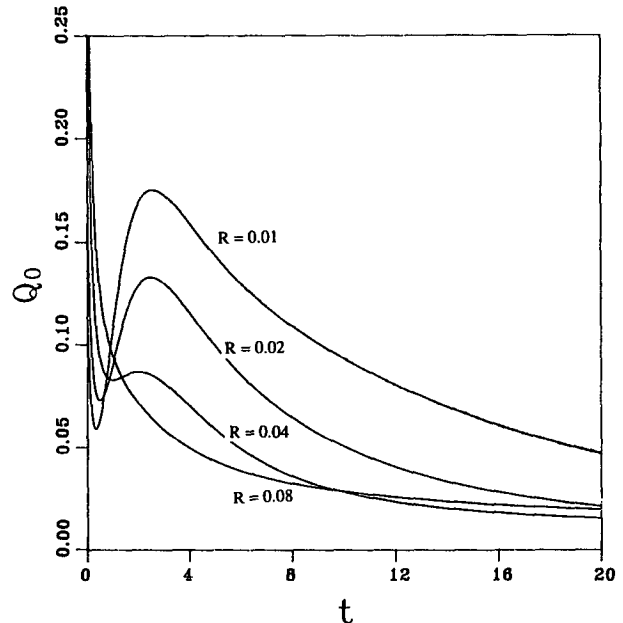

FIG. 9. The variation of horizontal density flux Q with time for different R.

When $t \ll a^2 K^{-1}$, the effects of the end walls on the diffusion process can be neglected and the exact solution of (3.5) for the initial condition (2.12) can be written as (Crank 1975)

$$b(x, t) = \frac{B}{\sqrt{\pi}} \int_{x/2|\overline{Kt}}^{\infty} \exp(-\eta^2) d\eta. \quad (3.7)^*$$

Therefore, $Q_0(R = \infty)$ corresponding to the pure diffusion case can be obtained using (3.6) as

$$Q_0(R = \infty) = -\frac{BH}{2} \left(\frac{K}{\pi t}\right)^{1/2}, \quad (3.8)^*$$

and the ratio $\Gamma = Q_0(R)/Q_0(R = \infty)$ can then be calculated from

$$\Gamma = -2\left(\frac{R}{\pi t}\right)^{-1/2} Q_0(R), \quad (3.9)$$

where the nondimensionalization has been made using K/UH, H/U, and UBH for R, T, and Q, respectively. Numerically calculated values of $Q_0(R)$ from (3.4) can be used to evaluate Γ in (3.9).

Linden and Simpson (1986) suggested that the horizontal density transport in the gravity current regime can be described as a Fickian process with a constant diffusion coefficient, let alone the turbulent diffusion regime. Based on the experimental results for $R > 0.04$, the effective diffusivity K^* was evaluated as

$$\frac{K^*(\text{Ri})}{K^*(\text{Ri} = 0)} = 1 + 0.22 \, \text{Ri}^{0.55}, \quad (3.10)^*$$

where $\text{Ri} = BH/q^2$ is a Richardson number based on the bubble rise velocity q of their experiments. The parameter Ri is not an independent parameter, but is related to R defined in (2.6) as

$$\text{Ri} \left(\equiv \frac{BH}{q^2}\right) = \left(\frac{l}{H}\right)^2 \left[\frac{(BH)^{1/2}H}{K}\right]^2 \quad (3.11)^*$$

$$= \left(\frac{l}{H}\right)^2 R^{-2}, \quad (3.12)^*$$

where l is the length scale of bubbles and $K = ql$. Using (3.12), (3.10) can be rewritten in terms of R as

$$\frac{K^*(R)}{K^*(R = \infty)} = 1 + 0.22\left(\frac{l}{H}\right)^{1.1} R^{-1.1}. \quad (3.13)^*$$

It is then possible to obtain Γ based on (3.8) as

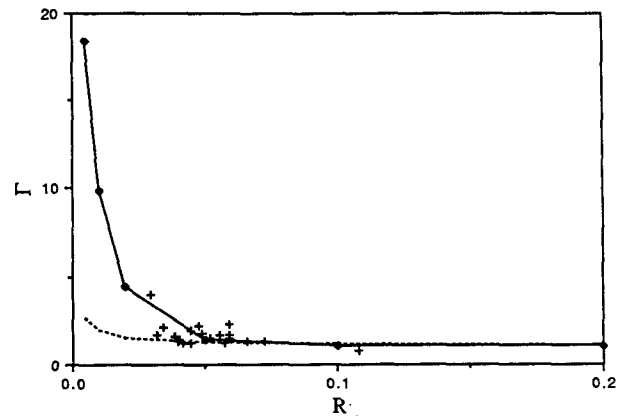$$\Gamma = \left[1 + 0.22 \left(\frac{l}{H}\right)^{1.1} R^{-1.1}\right]^{1/2}. \quad (3.14)$$

FIG. 10. The variation of Γ ($=$ the ratio of total horizontal transport of density to that by turbulent diffusion only) vs R.

In Fig. 10, numerical results for the variation of the ratio Γ with R are shown and are compared with the experimental results of Linden and Simpson (1986). Their empirical estimation (3.14) is also depicted by a dotted line. The numerical and the experimental results are in good agreement, but (3.14) clearly underestimates the horizontal density flux at small R. This suggests that the assumption of a Fickian process is not appropriate in describing the horizontal density flux in the gravity current regime.

b. Rotating case

Figures 11 and 12 show the density distribution, the streamlines, and the alongfrontal velocity field (v) for the cases $R = 0.01$ and 0.1, respectively, when $F = 1.0$ and $t = 5$. When $R = 0.01$ (Fig. 11), the propagation of the gravity current has been inhibited (cf. Fig. 3). Note that in Fig. 11b the flow direction is reversed. This suggests that the front moves backward at this moment, because, as will be seen later (Fig. 15a), the front is subjected to inertial oscillations. It is also observed that the streamlines are restricted to the frontal region and larger horizontal density gradients are observed in the outer region of the front. This pattern is similar to that observed during the geostrophic adjustment of a front of finite thickness (Ou 1984). In both sides of the density front, counterflowing alongfrontal currents are generated. As in the classical Rossby problem (Rossby 1937), the positions of the maximum alongfrontal velocities and the maximum horizontal density gradient at the fronts were found to coincide with each other. Further, at small R and large F, the motion is transformed into a three-cell circulation pattern as shown in Fig. 13, where the convergence and upwelling occur near the front. These phenomena also have been observed in the models of geostrophic fronts by Garrett and Loder (1981) and Ou (1984).
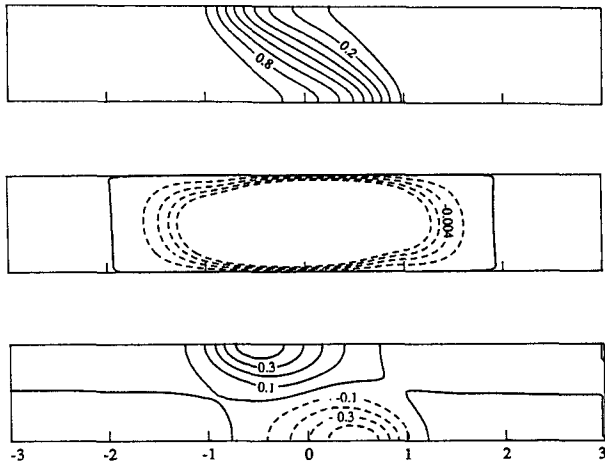
FIG. 11. (a) The density distribution $b(x, z)$: $t = 5$, $R = 0.01$, $F = 1.0$. (b) The streamlines of the flow $\psi(x, z)$: $t = 5$, $R = 0.01$, $F = 1.0$. (c) The along-frontal velocity field $v(x, z)$: $t = 5$, $R = 0.01$, $F = 1.0$.
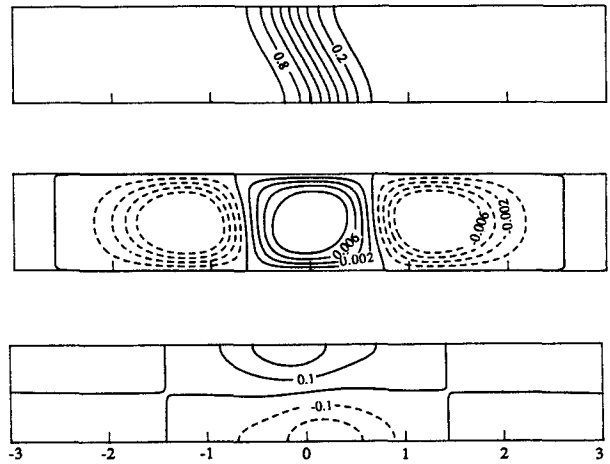

FIG. 13. (a) The density distribution $b(x, z)$: $t = 5$, $R = 0.01$, $F = 2.0$. (b) The streamlines of the flow $\psi(x, z)$: $t = 5$, $R = 0.01$, $F = 2.0$. (c) The alongfrontal velocity field $v(x, z)$: $t = 5$, $R = 0.01$, $F = 2.0$.

When $R = 0.1$, on the other hand, the effects of rotation are negligible for the density distribution, as can be seen by comparing Figs. 4 and 12, although the gravity current velocity has been reduced somewhat in comparison with the nonrotating case. This is also in agreement with the field observation of Nunes and Lennon (1987), who found that the earth's rotation becomes important only when the background turbulence level is weak. It was also observed that the along-frontal velocity field is much weaker here compared to the case $R = 0.01$. These observations are consistent with the variation of the frontal propagation
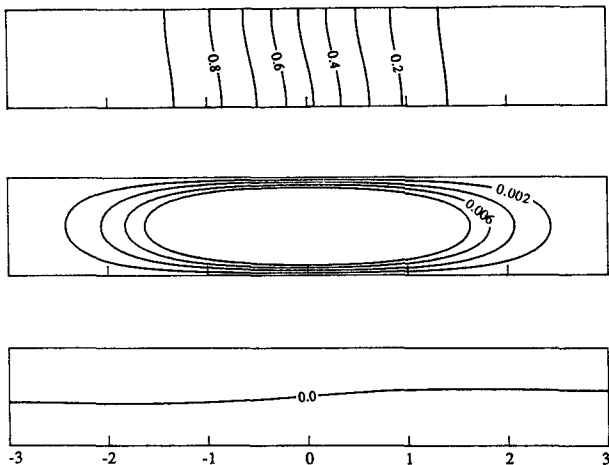

FIG. 12. (a) The density distribution $b(x, z)$: $t = 5$, $R = 0.1$, $F = 1.0$. (b) The streamlines of the flow $\psi(x, z)$: $t = 5$, $R = 0.1$, $F = 1.0$. (c) The alongfrontal velocity field $v(x, z)$: $t = 5$, $R = 0.1$, $F = 1.0$.

speeds with R and F. As shown in Fig. 14a, the frontal propagation is strongly inhibited by the rotation when $R = 0.01$, whereas it is hardly affected by the rotation when $R = 0.08$ (Fig. 14b).

In the presence of rotation, the cross-frontal velocity at the center $u_0 = u(x = 0, z = 0)$, initially driven by the density difference across the front, goes through a sequence of inertial oscillations (with the inertial frequency $2\pi/F$) with decaying amplitude. The corresponding velocities for $R = 0.01$ and 0.08 are shown in Figs. 15a and 15b, respectively; the broken lines indicate the predicted average velocity (over an inertial cycle) from the idealized model, which will be discussed in the following. A remarkable distinction between the cases with and without background turbulence is that, in the former case, the fluid motion does not attain the geostrophic equilibrium with time, and a cross-frontal velocity persists indefinitely. It is expected that the horizontal pressure gradient in (2.1) decreases with time owing to the horizontal diffusion of density, thus making it impossible to maintain the geostrophic equilibrium.

If the inertial and friction terms are neglected in (2.1) and (2.2), that is, $FL/U \gg 1$ and $FL^2/R \gg 1$, where L is the length scale of the horizontal variation of u, (2.1) and (2.4) can be combined to give

$$\frac{\partial^2 u}{\partial t^2} + F^2 u = -\frac{1}{\rho_0} \frac{\partial}{\partial t}\left(\frac{\partial p}{\partial x}\right). \qquad (3.15)$$

If hydrostatic equilibrium is assumed in (2.2) with vertically uniform b, (3.15) can be rewritten as

$$\frac{\partial^2 u}{\partial t^2} + F^2 u = -\frac{\partial}{\partial t}\left(\frac{\partial b}{\partial x}\right). \qquad (3.16)$$
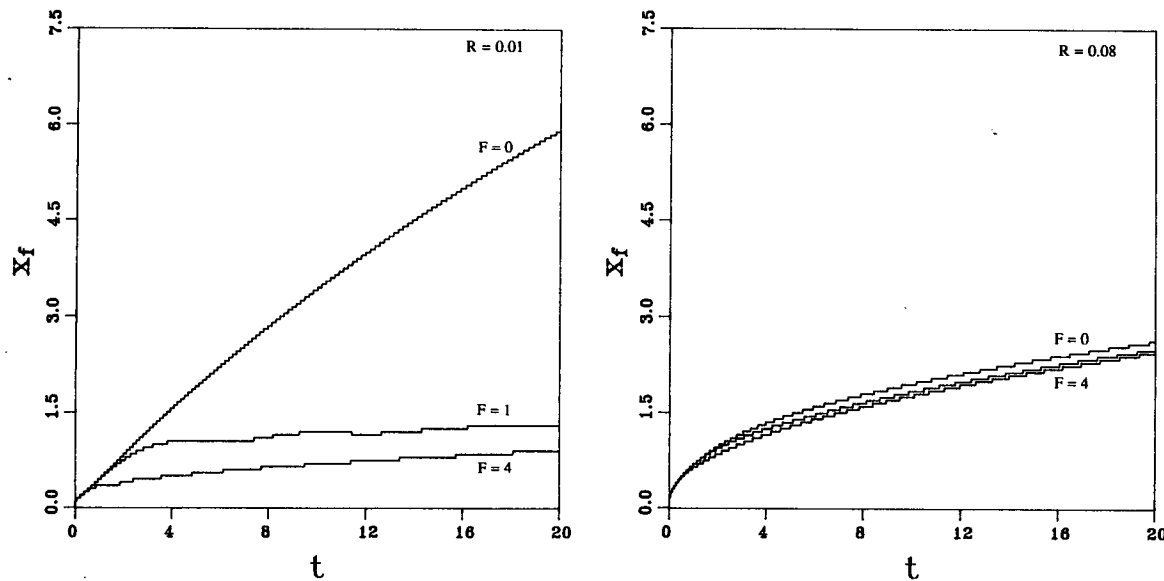
FIG. 14. The propagation of the front x_f with time t: (a) $R = 0.01$, (b) $R = 0.08$.

Finally, $\partial^2 u / \partial t^2$ can be neglected by considering the averaged quantity over the time scale of an inertial cycle and b can be estimated using (3.7). Thus, the cross-frontal velocity u_0 can be obtained as

$$u_0 = \frac{1}{4\sqrt{\pi R}} \frac{1}{F^2} t^{-3/2}. \qquad (3.17)$$

The velocities obtained from (3.17) are shown by the broken lines in Fig. 15a,b. When $R = 0.01$, (3.17) satisfactorily predicts the cross-frontal velocity averaged over an inertial cycle (Fig. 15a), but it underestimates u_0 significantly when $R = 0.08$ (Fig. 15b). When R is large, the shear stress terms are important and the Coriolis force does not become large enough to achieve
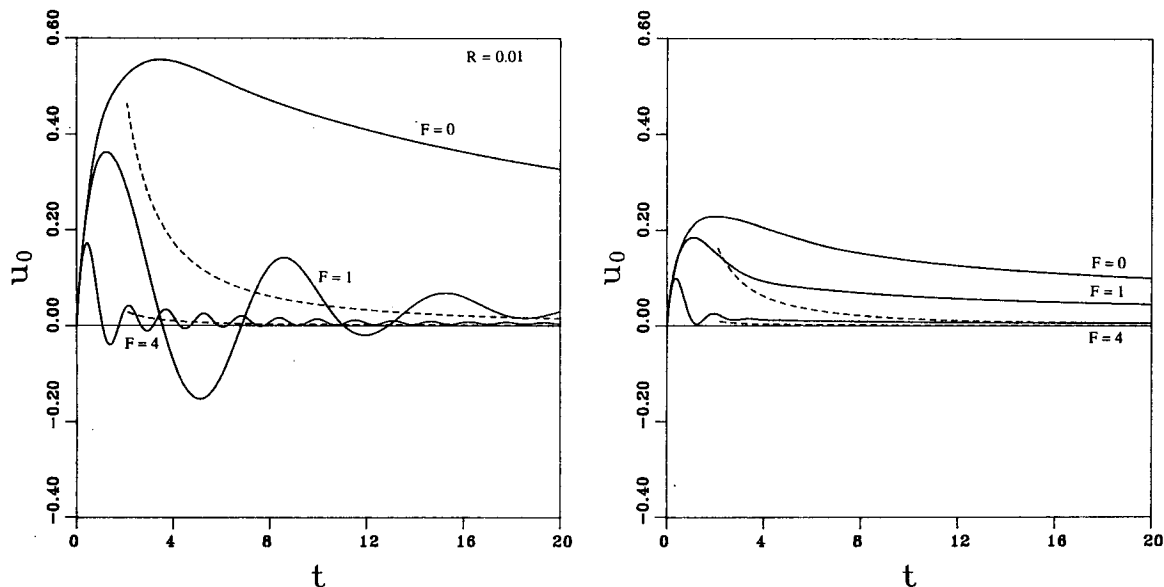

FIG. 15. The variation of the cross-frontal velocity u_0 with time: (a) $R = 0.01$, (b) $R = 0.08$.
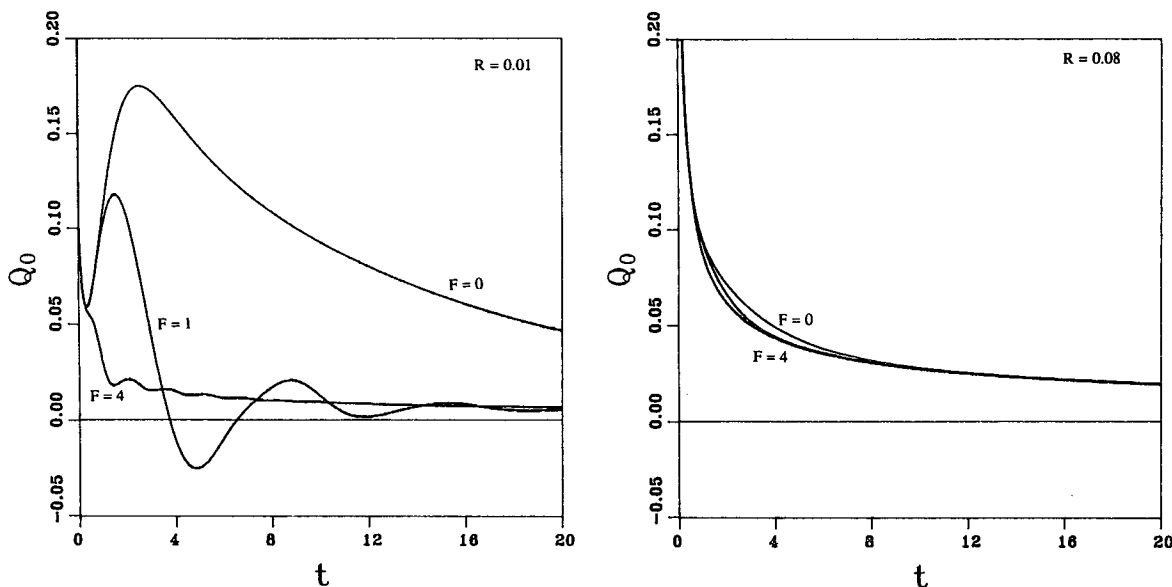The broken lines indicate the predictions of (3.17).

FIG. 16. The variation of the horizontal density flux with time: (a) $R = 0.01$, (b) $R = 0.08$.

the geostrophic balance, as evident from the very weak alongfrontal velocity field depicted in Fig. 12c.

Figs. 16a,b show the variations of horizontal density fluxes with time for different F and for $R = 0.01$ and 0.08, respectively. Again they show that the horizontal buoyancy flux is strongly reduced by the rotation at small R ($R = 0.01$), whereas it is hardly influenced by the rotation at large R ($R = 0.08$). It was found, however, that the value of Γ is close to unity regardless of R for both $F = 1.0$ and 4.0 cases. This implies that, even at small R, the horizontal flux due to cross-frontal flow u_0 is much smaller than that due to turbulent diffusion.

4. Summary and discussion

In this paper, a numerical model was presented to study the effects of background turbulence on gravity currents produced by lock exchange, both for rotating and nonrotating cases. It was shown that, in a nonrotating system, the transition from the gravity current regime to the turbulent diffusion regime takes place with the increase of the parameter R [$=K/(BH)^{1/2}H$]. It was found that the transition between two regimes occurs at $R \sim 0.04$. The variation of the propagation of the front, the horizontal density flux, the frontal thickness, and the potential energy anomaly have been calculated for different R, and the results were found to be consistent with the experimental results of Linden and Simpson (1986). It was further found that the transition between the two regimes is rather gradual, and the assumption of Fickian diffusion in estimating the horizontal buoyancy flux in the gravity current re-

gime cannot be justified, at least within the accuracy of the numerical model; these results are at variance with the postulations of Linden and Simpson (1986), and possible reasons for this discrepancy were provided.

Although in a rotating system the propagation of the front is inhibited by the Coriolis force, it was found that the geostrophic equilibrium cannot be achieved as a result of the horizontal diffusion of density. The cross-frontal velocity persists indefinitely, but its contribution to the horizontal density flux is small compared to that by the turbulent diffusion. The effects of rotation on the propagation of the front and the horizontal density flux were found to be impaired with increasing R.

To facilitate the comparison with field data, it is appropriate to modify the parameter R as

$$R \left(\equiv \frac{K}{(BH)^{1/2}H} \right) \approx \frac{K}{(10B_x\delta H)^{1/2}H} \quad (4.1)$$

$$\approx (H/10\delta)^{1/2}R^*, \quad (4.2)$$

where $R^* \equiv K/(B_x^{1/2}H^2)$ and the buoyancy difference between the two fluids B were estimated by using $B = 10\delta B_x$. Since $\delta/H \sim 0.5$ at $R = 0.04$ (Fig. 5), it is expected that the transition to occur at $R^* \sim 0.1$.

The degree of stratification in estuaries varies considerably with time. For example, in an analysis of the data taken from the Columbia River estuary, Jay and Smith (1988) observed that during spring tides the estuary is well mixed, whereas a two-layer stratification with strong frontal features appears during neap tides. The stratification appears in the estuary when the es-

timated vertical eddy diffusivity is of the order 0.1 $m^2 s^{-1}$. The typical depth and buoyancy scales for this estuary are estimated to be $H \sim 15$ m and $B_x \sim 10^{-5} s^{-2}$, thus yielding $R^* \sim 0.1$. Similarly, Nunes and Lennon (1987) observed the onset, development, and breakdown of stratification depending on the tidal characteristics in Spencer Gulf, South Australia. They suggested that the rate of change of potential energy anomaly should be given by

$$\frac{\partial \phi}{\partial t} = P - E, \qquad (4.3)*$$

where P is a source term due to the buoyancy flux and E is the rate of turbulent kinetic energy supply by winds and tidal stirring. They found that no significant stratification exists when $E > 3 \times 10^{-8} m^2 s^{-3}$. The terms on the rhs of (4.3) can be expressed using (2.5) as

$$P = -\frac{1}{H} \frac{\partial}{\partial x} \int_0^H ubz dz, \qquad (4.4)*$$

$$E = \frac{K \Delta B}{H}, \qquad (4.5)*$$

where $\Delta B = B(H) - B(0)$, and the horizontal diffusion and vertical advection terms are neglected. Since $\Delta B \sim 10^{-5}$ m s^{-2} and $H \sim 20 - 30$ m, K can be estimated as $K \sim 0.05$ $m^2 s^{-1}$ from (4.5). This gives the critical R^* number as $R^* \sim 0.1$, where the typical value of $B_x \sim 5.0 \times 10^{-7} s^{-2}$ was used.

The preceding estimate of critical R^* based on field observations is roughly of the same order as what is expected from the numerical model. However, it should be borne in mind that the present model is based on a highly idealized laboratory experiment designed to mimic natural flow situations, and care should be taken in extrapolating the model predictions to real estuarine situations. For example, estuarine eddy diffusivities are not constant, but vary spatially depending on the stratification and physical dimensions of the estuary. As a result of the reduction of eddy viscosity due to stratification and low aspect ratio, in general, critical R^* for estuaries is expected to be smaller. The topographic effects and river runoff are additional factors that need to be considered. Further, it is noted that the values of B and H considered here are for estuarine cases, and their magnitudes are larger for coastal fronts.

Finally, it should be noted that important three-dimensional features such as wavelike disturbances due to frontal instability (Griffith 1986) can develop, which cannot be captured from the present two-dimensional model. James (1981) showed that high values of K tend to suppress the wavelike disturbances at the front. More detailed physical and numerical models are required, however, to further understand the motion of fronts in the presence of rotation and background turbulence.

REFERENCES

Bowden, K. F., 1983: *Physical Oceanography of Coastal Waters,* Ellis Horwood, 30 pp.
Blumberg, A. F., and G. L. Mellor, 1987: A description of a three-dimensional coastal ocean model. *Three-Dimensional Coastal Ocean Models,* N. S. Heaps, Ed., Amer. Geophys. Union, 1–16.
Crank, J., 1975: *The Mathematics of Diffusion,* Clarendon Press, 313 pp.
Csanady, G. T., 1971: On the equilibrium shape of the thermocline in a shore zone. *J. Phys. Oceanogr.,* **1,** 263–270.
Daly, B. J., and W. E. Pracht, 1964: Numerical study of density current surges. *Phys. Fluids,* **11,** 15.
Droegemeier, K. K., and R. B. Wilhelmson, 1987: Numerical simulation of thunderstorm outflow dynamics. Part I: outflow sensitivity experiments and turbulence dynamics. *J. Atmos. Sci.,* **44,** 1180–1210.
Fedorov, K. N., 1986: *The Physical Nature and Structure of Ocean Fronts: Coastal and Estuarine Studies Monograph Series.* Springer-Verlag, 41–58.
Garrett, C. J. R., and J. W. Loder, 1981: Dynamical aspects of shallow sea front, *Philos. Trans. Roy. Soc. London,* **A302,** 563–581.
Garvine, R. W., and J. D. Monk, 1974: Frontal structure of a river plume. *J. Geophys. Res.,* **79,** 2251–2259.
Griffiths, R. W., 1986: Gravity currents in rotating systems. *Ann. Rev. Fluid Mech.,* **18,** 59–89.
——, and P. F. Linden, 1982: Laboratory experiments on fronts. *Geophys. Astrophys. Fluid Dyn.,* **19,** 159–187.
Haase, S. P., and R. K. Smith, 1989: The numerical simulation of atmospheric gravity currents. Part I: Neutrally stable environments, *Geophys. Astrophys. Fluid Dyn.,* **46,** 1–33.
James, I. D., 1981: Fronts and shelf circulation models. *Philos. Trans. Roy. Soc. London,* **A302,** 597–604.
——, 1984: A three-dimensional numerical shelf-sea front model with variable eddy viscosity and diffusivity. *Contin. Shelf Res.,* **3,** 69–98.
Jay, D. A., and J. D. Smith, 1988: Residual circulation and classification of shallow, stratified estuaries. *Physical Process in Estuaries,* J. Dronkers and W. van Leussen, Eds., Springer-Verlag, 21–41.
Kao, T. W., C. Park, and H. P. Pao, 1977: Buoyant surface discharge and small-scale oceanic fronts: A numerical study. *J. Geophys. Res.,* **82,** 1747–1752.
——, ——, and ——, 1978: Inflows, density currents and fronts. *Phys. Fluids,* **21,** 1912–1922.
Linden, P. F., and G. J. F. van Heijst, 1984: Two-layer spin-up and frontogenesis. *J. Fluid Mech.,* **143,** 69–94.
——, and J. E. Simpson, 1986: Gravity driven flows in a turbulent fluid. *J. Fluid Mech.,* **172,** 481–497.
McClimans, T. A., 1988: Estuarine fronts and river plumes. *Physical Process in Estuaries,* J. Dronkers and W. van Leussen, Eds., Springer-Verlag.
Noh, Y., and H. J. S. Fernando, 1991: Gravity current propagation along an incline in the presence of boundary mixing. *J. Geophys. Res.,* **96,** 12 586–12 592.
——, and ——, 1992: The motion of buoyant clouds along an incline

in the presence of boundary mixing. *J. Fluid Mech.*, **235**, 557–577.

Nunes, R. A., and G. W. Lennon, 1987: Episodic stratification and gravity currents in a marine environment of modulated turbulence. *J. Geophys. Res.*, **92**, 5465–5480.

Ou, H. W., 1984: Geostrophic adjustment: A mechanism for frontogenesis, *J. Phys. Oceanogr.*, **14**, 994–1000.

Ramming, H. G., and Z. Kowalik, 1980: *Numerical Modelling of Marine Hydrodynamics.* Elsevier, 1–22.

Rossby, C. G., 1937: On the mutual adjustment of pressure velocity distribution in certain simple current systems: I. *J. Mar. Res.*, **1**, 15–28.

Scorer, R. S., 1978: *Environmental Aerodynamics.* Ellis Horwood, 330–356.

Simpson, J. E., 1987: *Gravity Currents in the Environment and Laboratory.* Ellis Horwood.

Simpson, J. H., 1981: The shelf-sea fronts: Implications of their existence and behavior. *Philos. Trans. Roy. Soc. London*, **A302**, 531–546.

——, and J. D. James, 1986: Coastal and estuarine fronts. *Baroclinic Process on Continental Shelves*, C. N. K. Moores, Ed., Am. Geophys. Union, 63–94.

——, C. M. Allen, and N. C. G. Morris, 1978: Fronts on the continental shelf. *J. Geophys. Res.*, **83**, 4607–4614.

Thomas, N. H., and J. E. Simpson, 1985: Mixing of gravity currents in turbulent surroundings: Laboratory studies and modelling implications. *Turbulence and Diffusion in Stable Environments*, J. C. R. Hunt, Ed., Clarendon Press, 61–96.

van Heijst, G. J. F., 1985: A geostrophic adjustment model of a tidal mixing front. *J. Phys. Oceanogr.*, **15**, 1182–1190.

Walters, R. A., 1985: A tale of two estuaries: Columbia Bay, Alaska, and San Francisco Bay, California. *Estuarine Circulation.* B. J. Neilson, A. Kuo, and J. Brubaker, Eds., Humana Press, 183–201.

Wang, D. P., 1984: Mutual intrusion of a gravity current and density front formation. *J. Phys. Oceanogr.*, **14**, 1191–1199.

——, 1985: Numerical study of gravity current in a channel. *J. Phys. Oceanogr.*, **15**, 299–305.